

New Azo-Schiff Base Ligand Capped Silver and Cadmium Sulfide Nanoparticles Preparation, Characterization, Antibacterial and Antifungal Activities

A. Kakanejadifard^{a,*}, V. Khojasteh^a, A. Zabardasti^a and F. Azarbani^b

^aDepartment of Chemistry, Faculty of Science, Lorestan University, Khorramabad, Iran

^bDepartment of Biology, Faculty of Science, Lorestan University, Khorramabad, Iran

(Received 25 May 2018, Accepted 15 July 2018)

A novel azo-Schiff base ligand (L) was prepared by reacting 2-hydroxy-5-(pyridine-4-yl diazenyl)benzaldehyde with 1,2-phenylenediamine. Moreover, Silver nanoparticles (Ag-NPs) and Cadmium sulfide nanoparticles (CdS-NPs) were prepared using azo-Schiff base ligand (L) as capping and reducing agent. The solid-state fluorescence spectroscopy was used to investigate the interaction between L with one of the nanomaterials (CdS-NPs). The fluorescence studies showed that L suppresses the CdS-NPs fluorescence. The antibacterial and antifungal activities of the mentioned nanoparticles were determined against different bacteria and plant fungal strains and the obtained results were compared. The azo-Schiff base ligand (L) only exhibited antibacterial activity against *B. cereus* as Gram-positive bacterium. L-Ag-NPs had moderate to high antibacterial properties for both Gram-negatives and Gram-positives species. Moreover, L-CdS-NPs showed activity against *B. cereus* as a Gram-positive and *E. coli* as a Gram-negative bacterium. All the described compounds showed antifungal activity against the fungal strains tested.

Keywords: Azo-Schiff base, Antibacterial and antifungal activity, CdS nanoparticles, Ag nanoparticles

INTRODUCTION

Azo-Schiff bases have many biological activities such as antibacterial, antifungal, and antitumor activities [1,2]. Schiff bases capped-nanoparticles, their antibacterial activity is more than that of Schiff bases alone [3]. Studies on the Schiff base nanomaterials are among the least areas of nanoscience investigations and joining Schiff bases to nanoparticles may result in numerous pharmaceutical applications [4]. Due to the wide range applications of nanostructures, they have received considerable attention, especially in biology [5,6]. Silver and its compounds have an inhibitory effect on bacteria, fungi, and viruses [7-9]. Silver nanoparticles (SNPs) synthesized with different methods have shown good antibacterial and antifungal

properties that can be used in different fields such as burn dressings, water purification systems, and medical devices [10].

Although nanoparticles can be synthesized by different methods, most of them need complicated equipment and suffer from long reaction time. Besides, stabilizing and reducing agents are necessary for the synthesis of nanoparticles [11-16].

Cadmium sulfide (CdS) is a popular II-VI semiconductor with a 2.42 eV band gap at ambient temperature and has many applications in gas sensors, photochemical catalysis, infrared solar cells, detectors for laser, nonlinear optoelectronic devices, luminescence devices, optical, and biological materials [17-19].

Cadmium sulfide nanoparticles (CdS-NPs) are also fluorescent. The light emitting properties of CdS-NPs have been among the most studied properties in quantum dots

*Corresponding author. E-mail: kakanejadi.a@lu.ac.ir

and are of growing interest as emissive materials in light-emitting devices [20]. Fluorescence quenching refers to any process that decreases the fluorescence intensity of a given substance. A variety of processes can result in quenching, such as excited state reactions, energy transfer, complex-formation and collisional quenching. As a consequence, quenching is often heavily dependent on pressure and temperature. Quenching and dequenching upon interaction with a specific molecular biological target is the basis for activatable optical contrast agents for molecular imaging.

The synthetic routes for preparation and conjugation of NPs to capping agent require severe conditions. Hence, in the present study in continuation of our recent work on interaction of azo-Schiff base with nanomagnetic compounds, graphene and graphene oxide [21,22], we decided to synthesize and characterize the azo-Schiff base ligand [2,2'-((1,2-phenylene bis(azanylylidene))bis(methanylylidene))bis(4-(pyridin-4-yl diazenyl)phenol)], L-Ag-NPs and L-CdS-NPs with simple methods and without using any additional stabilizing and reducing agent.

Indeed, numerous applications of azo-Schiff base and conjugated nanoparticles in various material science areas were the motivation of this research work. The purpose of using the mentioned ligand is 1) easy preparation of the ligand, and 2) presence of the phenolic hydroxy group in its structure that obviates the need for an additional reducing agent. In order to investigate the fluorescence properties of the prepared nanostructures, we used CdS-NPs and evaluated the interaction of newly synthesized compounds using fluorescence spectroscopy. We characterized the morphology and the average size of particles by X-ray diffraction (XRD), scanning electron microscope (SEM), dynamic light scattering (DLS), and atomic force microscopy (AFM). The antibacterial and antifungal behavior of newly synthesized compounds was also evaluated for various groups of both bacteria and plant fungi, and the results were compared with each other.

EXPERIMENTS

Materials

All materials were used as received and obtained from

Merck company. Analytically reagent grade solvents were used in the reactions. The pathogenic strains used in this study, including *Escherichia coli* (*E. coli*, PTCC 1330) and *Klebsiella pneumoniae* (*K pneumoniae*, PTCC 1035) as Gram-negative bacteria and *Staphylococcus aureus* (*S aureus*, PTCC 1112), *Bacillus cereus* (*B cereus*, PTCC 1556) as Gram-positives were obtained from Pasteur Institute of Iran. The plant fungal strains (*Fusarium oxysporum*, *Alternaria solani*, *Pythium aphanidermatium*, and *Macrophomina phaseolina*) were prepared from phytopathology center of agriculture department and natural resources of Lorestan University (Iran). The azo compounds of 2-hydroxy-5-((E)-pyridine-4-yl diazenyl)benzaldehyde (1) were prepared by reaction of 2-hydroxybenzaldehyde and 4-aminopyridine according to the published papers [23-25].

Instruments

Measuring the melting points was achieved with Electrothermal 9200 system. Infrared spectra at 4000-400 cm^{-1} using KBr discs were obtained on FT-IR spectrophotometer Shimadzu 8400 S. A Bruker DRX-400 MHz Advanced NMR spectrometer with the hydrogen assignments was used to determine the ^1H and ^{13}C NMR spectra in DMSO- d_6 as a solvent. The electronic spectra with a Shimadzu 6405 spectrophotometer were recorded in dimethylformamide (DMF) solvent. A LEO 440i scanning electron microscope (SEM) (MIRA3-LMU) was used to assess morphologies of tested samples. An energy dispersive X-ray spectroscopy (EDX) (DXP-X10P) at an acceleration voltage of 15 kV was applied to determine the composition of prepared samples. For SEM analyses, the dried powder of samples was placed on an adhesive tape stuck on a metallic stub and by sputtering for 15s, a thin layer of gold was coated on them. An AFM FULL PLUS-Noncontact model was used to perform the atomic force microscopy (AFM). XRD patterns of nanomaterials for 2θ (10° to 80°) were obtained using a Holland Panalytical X'PertPro diffract meter with wavelength of x-ray beam (Cu $K\alpha$): 1.54 angstrom at a scanning speed of $2^\circ/\text{min}$. Dynamic Light Scattering (DLS) was performed using a 90 plus particle size analyzer equipped with a diode laser operating at 658.0

nm to determine the size distribution of synthesized nanomaterials. The emission spectra of ligand and ligand-capped cadmium sulfide nanoparticles in the solid state were recorded using a Varian Cary Eclipse Fluorescence Spectrophotometer. Slits with 5.0 nm bandpass were used for emission and excitation. The spectra were obtained in the range of 350-650 nm and the excitation wavelength was 350 nm. The processes were accomplished at ambient temperature.

Synthesis

Synthesis of 2,2'-((1,2-phenylene bis(azanylylidene))bis(methanylylidene))bis(4-(pyridin-4-ylidiazanyl) phenol), azo-Schiff base (L). To a stirring ethanolic solution of 2-hydroxy-5-(pyridine-4-ylidiazanyl) benzaldehyde (1, 2.27 g, 10 mmol, 130 ml) and formic acid (0.25 g, 5.5 mmol, 98% aqueous solution) an ethanolic solution of 1,2-phenylenediamine (2, 0.54 g, 5 mmol, 20 ml) was added and the mixture was refluxed for 5 h. The progress of the reaction was monitored through TLC with methanol/hexane ratio 9/1. After evaporation of the solvent, the solid product was separated and recrystallized with CH₃CN/MeOH ratio 2/1, and air dried.

Synthesis of L-Ag-NPs. To a stirring ethanolic solution of 2-hydroxy-5-(pyridine-4-ylidiazanyl)benzaldehyde (1, 1.5 g, 6 mmol, 130 ml) and formic acid (0.25 g, 5.5 mmol, 98% aqueous solution), an ethanolic solution of 1,2-phenylenediamine (2, 0.54 g, 3 mmol, 20 ml) and a certain amount of AgNO₃ (3×10^{-3} M) were added. The mixture was refluxed for 5 h, then the solvent was evaporated and the yellowish brown solid was washed with absolute ethanol and double distilled water to remove the unreacted materials, and then air dried.

Synthesis of L-CdS-NPs. To synthesize CdS-NPs, the method reported in the literature [7] was used. To a stirring methanolic solution of Cd(CH₃COO)₂·2H₂O (10 ml, 3×10^{-3} M) an appropriate concentration of the methanolic solution of Na₂S·9H₂O was added. Then, 9×10^{-3} M solution of the synthesized ligand in MeOH (10 ml) was prepared. The two solutions were mixed, stirred, and then the formed precipitate solution was poured into a round bottom flask and sonicated. After 1 h, the CdS sediment was filtered off,

washed with absolute ethanol and double distilled water to remove the unreacted materials, and then air dried. Uncapped CdS was prepared with similar procedure.

ANTIBACTERIAL AND ANTIFUNGAL ACTIVITIES

Pathogenic Strains

In this study, the synthesized compounds were examined against *K. pneumonia* (PTCC 1035), *E. coli* (PTCC 1330) as Gram negatives, *S. aureus* (PTCC 1112) *B. cereus* (PTCC 1556), as Gram-positive bacteria, and plant fungi (*Fusarium oxysporum*, *Alternaria solani*, *Pythium aphanidermatum*, and *Macrophomina phaseolina*).

Antibacterial Activity

The synthesized ligand and L-Ag-NPs were assayed for their antibacterial activities through agar well diffusion method [26]. Fresh bacteria cultures were used for inoculation of Muller Hinton agar plates. Wells with 7 mm diameters were dug by a sterile cork borer in solidified agar. DMSO was used to dissolve the compounds and the wells were filled with 60 µl of their solution. DMSO as a dissolving agent was tested as a control. To allow the diffusion, plates were left for 2 h in the refrigerator and then incubated for 24 h at 37 °C. Amikacin was the reference antibiotic in this test. The antibacterial properties of the mentioned compounds were determined by measuring the inhibition zone around the well.

Antibacterial behaviors of L, L-CdS-NPs, and uncapped CdS-NPs against mentioned bacteria were screened by paper disk method [27]. We used 24 h cultures of bacteria for inoculation of nutrient agar plates. The concentration of 30 µg/disk of dissolved compounds in DMSO was placed on the inoculated plates. The standard antibiotic was Amikacin. The zone of inhibition diameter was measured (mm) after 24 h incubation at 37 °C.

Antifungal Activity

The antifungal activities of the sensitized L, L-Ag-NPs, and L-CdS-NPs were measured by agar dilution method [28] and inhibition percentage against the mycelia growth

diameter was expressed. The fungal strains for experiment including *Fusarium oxysporum*, *Alternaria solani*, *Pythium aphanidermatum*, and *Macrophomina phaseolina* were separated from their different host plants. These pathogens were further purified in water agar medium with hyphal tip and single spore methods. Before the experiment, they were cultured for 4 days at 25 °C on potato dextrose agar (PDA). Each diluted solution (1 ml) was mixed with PDA (10 ml) and then put in the petri dish. Finally, the spores from a mycelia disk (5 mm in diameter) were put on the middle part of the PDA plate. All plates were put into an incubator (25 °C) until fungal colony in the control petri dish (DMSO) cover the whole surface of the petri dish. This experiment was replicated four times in a thoroughly random model. The obtained statistical data were analyzed by SAS 9.1 software. In order to the investigate antifungal properties of newly synthesized L and L-capped nanoparticles, the percentage of Mycelial zone inhibition was calculated [29] using the following formula:

$$IP = \frac{dc - dt}{dc} \times 100$$

where IP is a percentage of Mycelial zone inhibition and dt and dc are average diameters (mm) of the mycelia colonies of the treated sets and control, respectively.

RESULTS AND DISCUSSION

Rational design, synthesis and applications of new azo-Schiff base (L) are our main interests. To this end, we synthesized new azo-Schiff base (L), L-Ag-NPs, and L-CdS-NPs and investigated their antibacterial and antifungal activities. The air-stable ligand of 2,2'-((1,2-phenylene bis(azanilylidene))bis(methanilylidene))bis(4-(pyridin-4-ylidiazanyl)phenol) was prepared by condensation reaction of 2-hydroxy-5-(pyridine-4-ylidiazanyl)benzaldehyde (1) and 1,2-phenyldiamine in ethanol.

Synthesis of L-Ag-NPs was done by refluxing condition in ethanol. The azo-Schiff base incorporation with silver nanoparticles was achieved via the reduction of AgNO₃ salt and used for CdS-NPs sonochemical bath. Interaction of metal ion with azo-Schiff base occurs by chelation with

donor atoms of the ligand. We believe that OH groups, in addition to using ethanol as the solvent, will enhance the reducing activity of azo-Schiff base ligand for Ag⁺ ions. Also, the presence of imine group in ligand structure increases the interaction of ions (Ag⁺, Cd²⁺) by complex formation.

Characterization

Spectroscopic methods such as mass, FT-IR, UV-Vis, and NMR were used to characterize azo-Schiff base (L). D₂O exchangeable signal for phenolic OH groups of L appeared at 13.65 ppm and the CH=N proton showed signal at 8.84 ppm in ¹H NMR spectrum. Azo unit of pyridine ring exhibited signals at 8.81-8.79 ppm (4H, d, J = 6) and 7.74-7.72 ppm (4H, d, J = 6.4). The other ring containing OH group showed signals at 8.00-7.97 ppm (2H, dd, J = 8.8, J = 2.4), 7.14-7.12 ppm (2H, d, J = 9.2), and 7.70-7.69 ppm (2H, d, J = 3.2). Two doublets at 7.32-7.31 ppm and 7.29-7.28 ppm (4H, d, J = 9.6) (Figs. S5 and S6) appeared for the protons of the phenyl ring of the prepared compound. The ¹³C NMR of L exhibited signals at 163.82 ppm, 157.51 ppm, and 151.82 for Ar-C-OH, CH=N, and -C-N=N, respectively. All the other aromatic carbon shifts can be seen at 144.18-114.42 ppm (Figs. S7 and S8).

The FT-IR spectra of the synthesized L, L-Ag-NPs, and L-CdS-NPs in the range of 4000-450 cm⁻¹ at ambient temperature are presented in (Fig. 2). In the solid-state FT-IR spectrum of azo-Schiff base, the OH stretching absorption bond of the compound is at 3564 cm⁻¹. ν(Ar-H) 3059, ν(CH=N) 2926, 2813, ν(C=N) 1625, ν(N=N) 1591, ν(C=C) 1494, ν(C-N) 1359, 1274, ν(C-O) 1161 were also observed in the spectrum.

Compared to L, for L-CdS-NPs and L-Ag-NPs shifting of the peaks with an increase in the intensity are observed. In the FT-IR spectrum of L-Ag-NPs, bands at 2925, 1560, 1350, 1271, 1191, 823, 748, 613, 574 and 503 cm⁻¹ are assigned to the formation of L-Ag-NPs (Fig. 2a). In L-CdS-NPs spectrum, the bands at 3380, 1587, 1485, 1271, 1161, and 1105 cm⁻¹ are related to OH, C=N, N=N, C-C, C-N and C-O stretching, respectively (Fig. 2b). The bands at 829 and 750 cm⁻¹ and the new weak peaks at 501 and 559 cm⁻¹ were observed that are not seen in the spectrum of L. In uncapped CdS-NPs, the strong absorption peaks at 3446, 1627, 1114, 1008 and 621 cm⁻¹ are attributed to the formation of

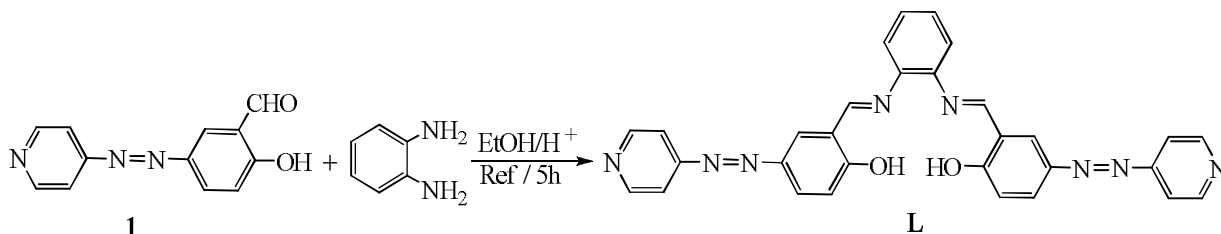


Fig. 1. Synthesis of 2,2'-((1,2-phenylene bis(azanylylidene))bis(methanylylidene))bis(4-(pyridine-4-yl)phenol).

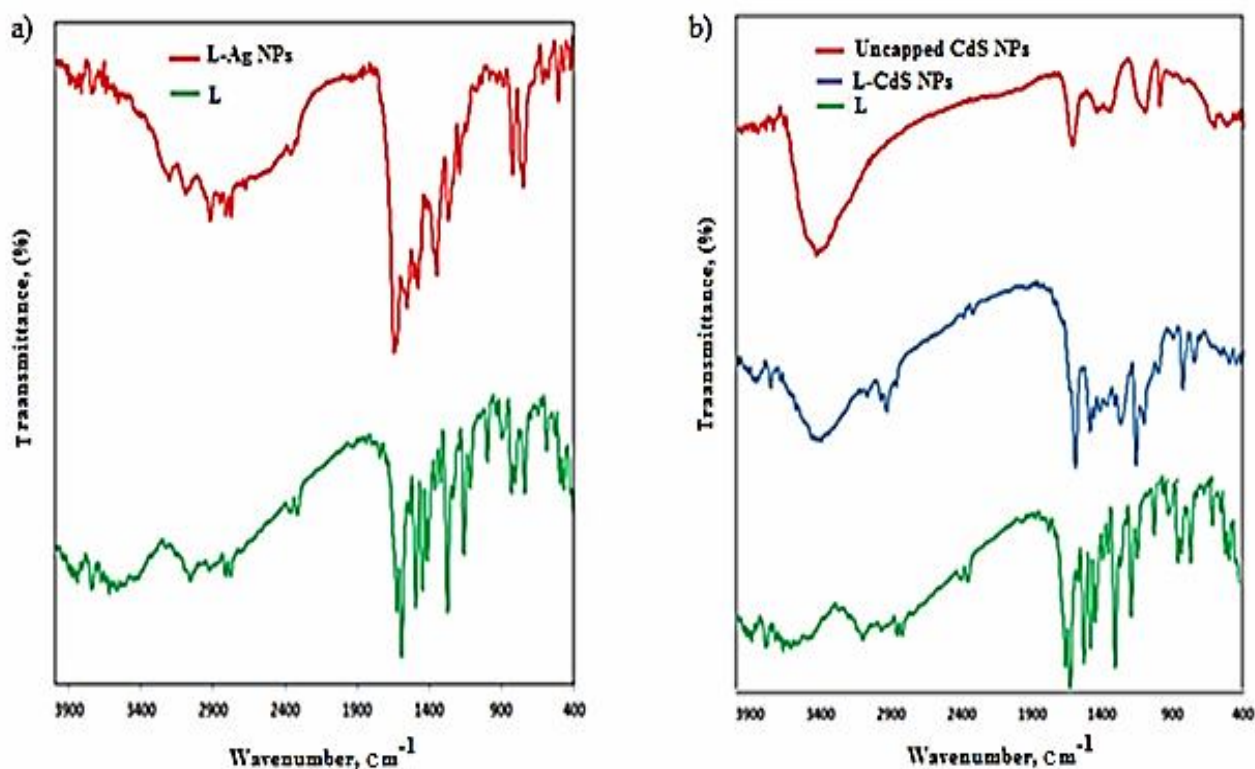


Fig. 2. FT-IR spectra of a) L, L-Ag-NPs, b) L, L-CdS-NPs and uncapped CdS.

cadmium sulfide nanoparticles. The differences between the FT-IR spectra of the L, L-CdS-NPs, and L-Ag-NPs may be attributed to coordination between ligand and Ag^+ and Cd^{2+} , indicating conjugation of the ligand to the cadmium sulfide NPs and silver NPs.

The electronic spectra of compounds were illustrated in (Fig. 3). For L, the maximum absorption band at 368 nm was assigned to $\pi \rightarrow \pi^*$ transition of N=N linkage and aromatic rings. Also, the $n \rightarrow \pi^*$ electronic transition

observed at 521 nm was attributed to the azo aromatic chromophore and intramolecular charge transfer interaction [23-25,30-33]. In L-Ag-NPs and L-CdS-NPs absorption spectra, two maximum absorption bands were observed at 362, 366, and 503, 516 nm (Fig. 3). In this case, the blue shift was found and absorption bands shifted to a lower wavelength, probably due to the effect of the size quantization. The decrease in particle size creates a blue shift [34].

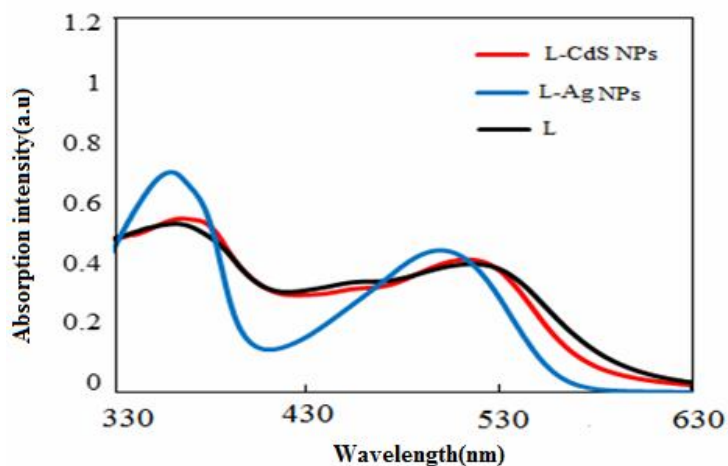


Fig. 3. UV spectra of a) L, L- Ag-NPs, b) L, L-CdS-NPs, and c) uncapped CdS-NPs.

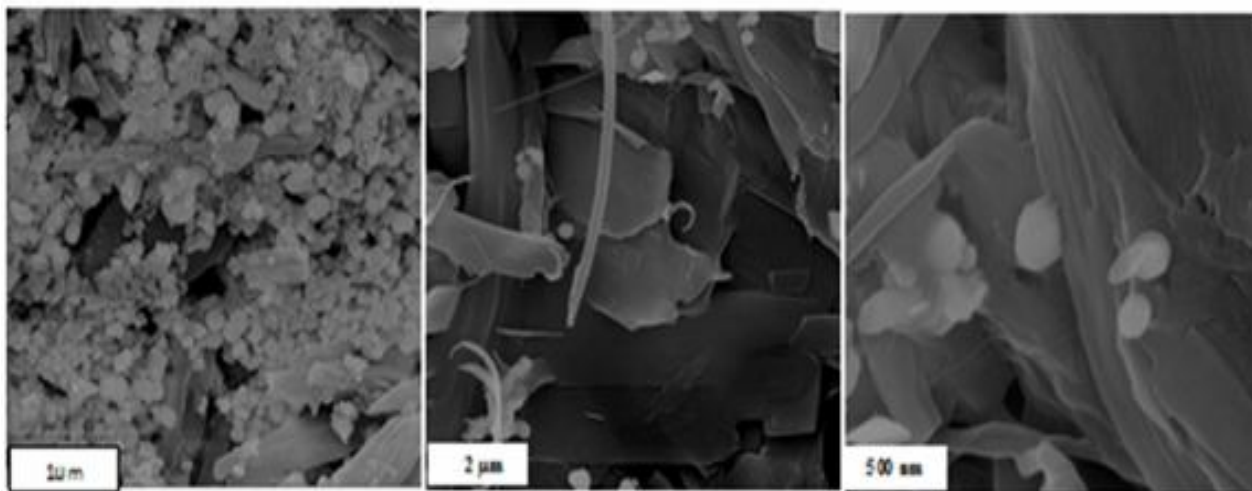


Fig. 4. SEM micrograph of L- Ag-NPs.

SEM was used for evaluation of the materials morphology. The SEM images, EDX with elemental maps for L-Ag-NPs, and L- CdS NPs are presented in (Figs. 4, 5, 6), respectively. The SEM image of L-Ag-NPs is presented in (Fig. 4). The figure exhibits the distribution of Ag-NPs inside ligand matrix that might be attributed to complexation between ligand and Ag^+ causing the formation of separate silver nanoparticles in ligand matrix. This result, in turn, is induced by the activity of silver cation with OH group in

ligand and ethanol solvent that can reduce the silver ion. The surface seems to be layered with the spherically formed silver nanoparticles. Moreover, due to aggregation, SNPs are not homogenous distribution on the matrix of ligand and the average size of the particles was estimated about 49 nm. As seen in the SEM image of L-CdS-NPs the morphology of the surface has different shapes with homogeneous distributions (Fig. 6a). The average size of L-CdS-NPs estimated by SEM was 30 nm, in accord with XRD results.

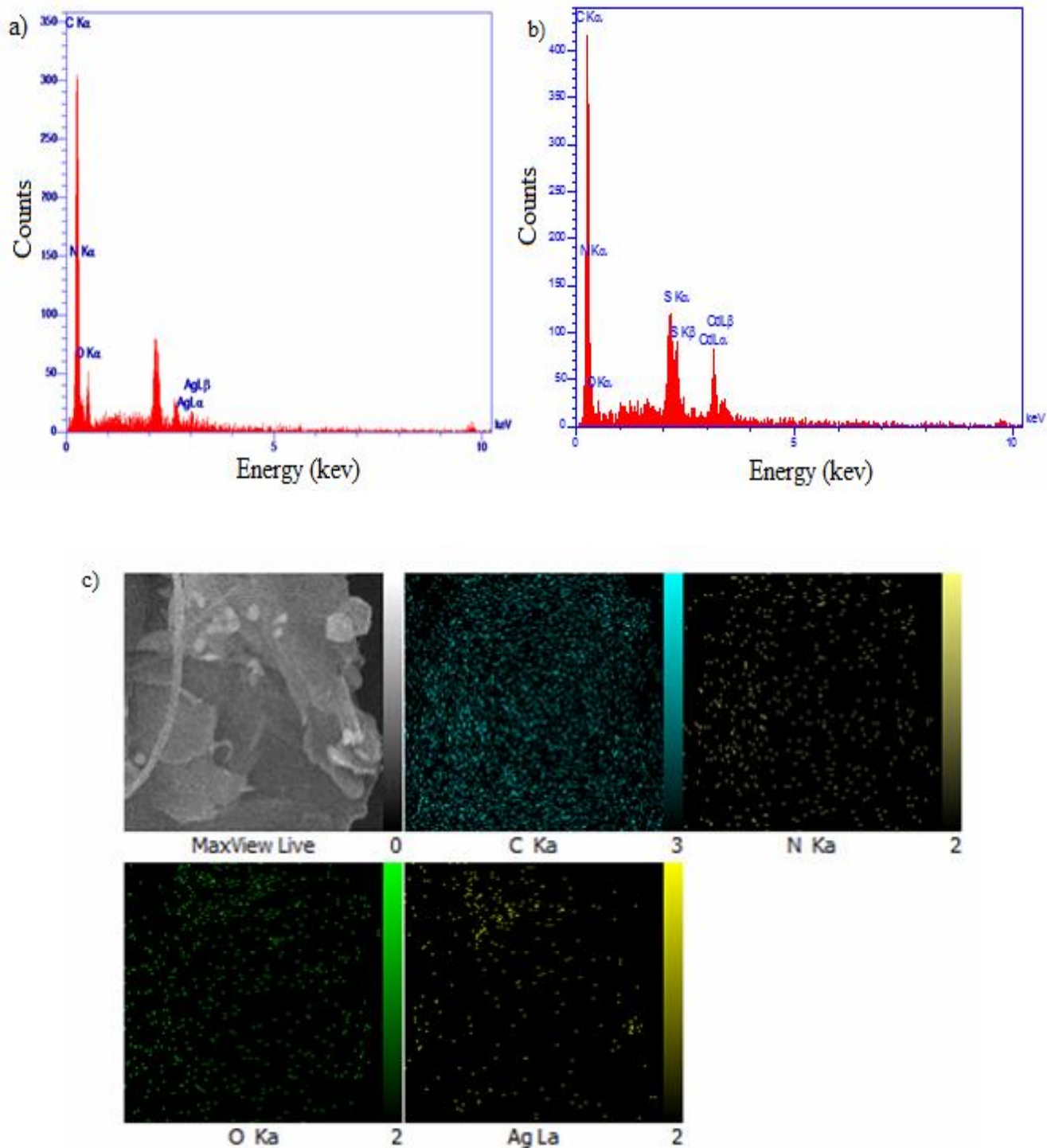


Fig. 5. a) EDX spectrogram, b) elemental maps of L-Ag-NPs, c) EDX spectrogram of L-CdS, NPs, and d) elemental maps of L-CdS-NPs.

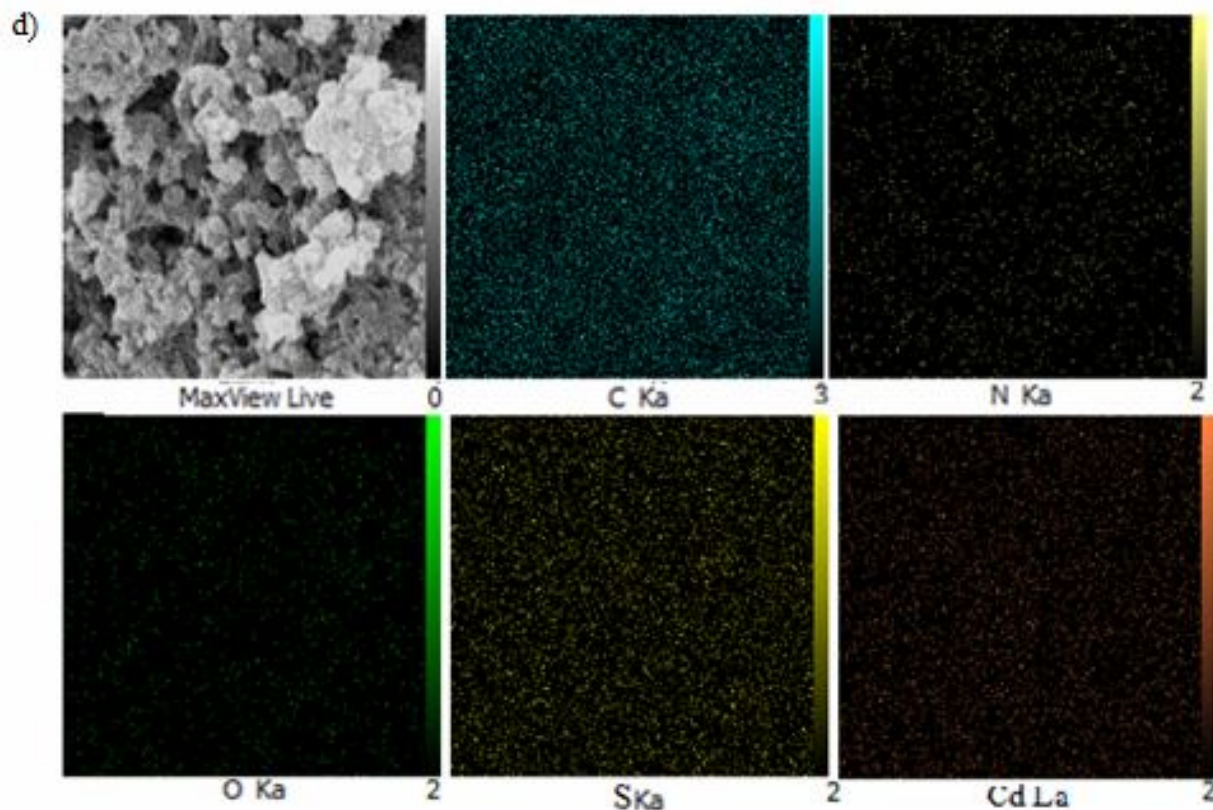


Fig. 5. Continued.

The EDX spectrum was used to determine the composition of Ag and CdS nanomaterials. EDX spectrum strongly proves the formation of nanoparticles, L-Ag-NPs (Fig. 5a), containing C, N, O, and Ag, L mainly generated C, N, and O peaks while the Ag peak was generated by Ag-NPs. As presented in (Fig. 5b), L-CdS-NPs contain C, N, O, S, and Cd. The peaks of C, N, and O are related to L and the peaks of S and Cd concern to the CdS -NPs. Elemental maps of the synthesized nanoparticles are shown in (Figs. 5c and 5d). Distribution of Cd and S in a matrix of ligand is homogenous, while Ag does not show a good distribution that may be due to aggregation.

The structural analysis of solid products was achieved using XRD. Figure 7 exhibits the XRD shape of L and L-capped nanoparticles. The XRD for L-Ag-NPs consists of four diffraction peaks at 2θ values of 38° , 44.5° , 65° and 77° confirming the crystalline structure of Ag-NPs with the (111), (200), (220) and (311) crystalline planes (Fig. 7a).

The XRD pattern of uncapped CdS-NPs exhibits four broad peaks at 2θ values of 27° , 44° , 52° and 72° with the (111), (220), (311) and (331) crystalline planes of CdS-NPs (Fig. 7b). The 2θ values are similar to those reported for CdS [35].

The XRD pattern of L-CdS-NPs exhibits only two weak peaks at 27° and 46° , suggesting that the product is poorly crystallized. The mean particle size of the sample was calculated by Debye-Scherrer equation formula:

$$D = \frac{k\lambda}{\beta \cos\theta}$$

where β is the full-width at half maximum (FWHM) and θ is the diffraction angle. K is a constant (shape factor), and λ is the wavelength of the X-ray.

The average particle sizes were determined about 28-30 nm for L-Ag-NPs and L-CdS, respectively.

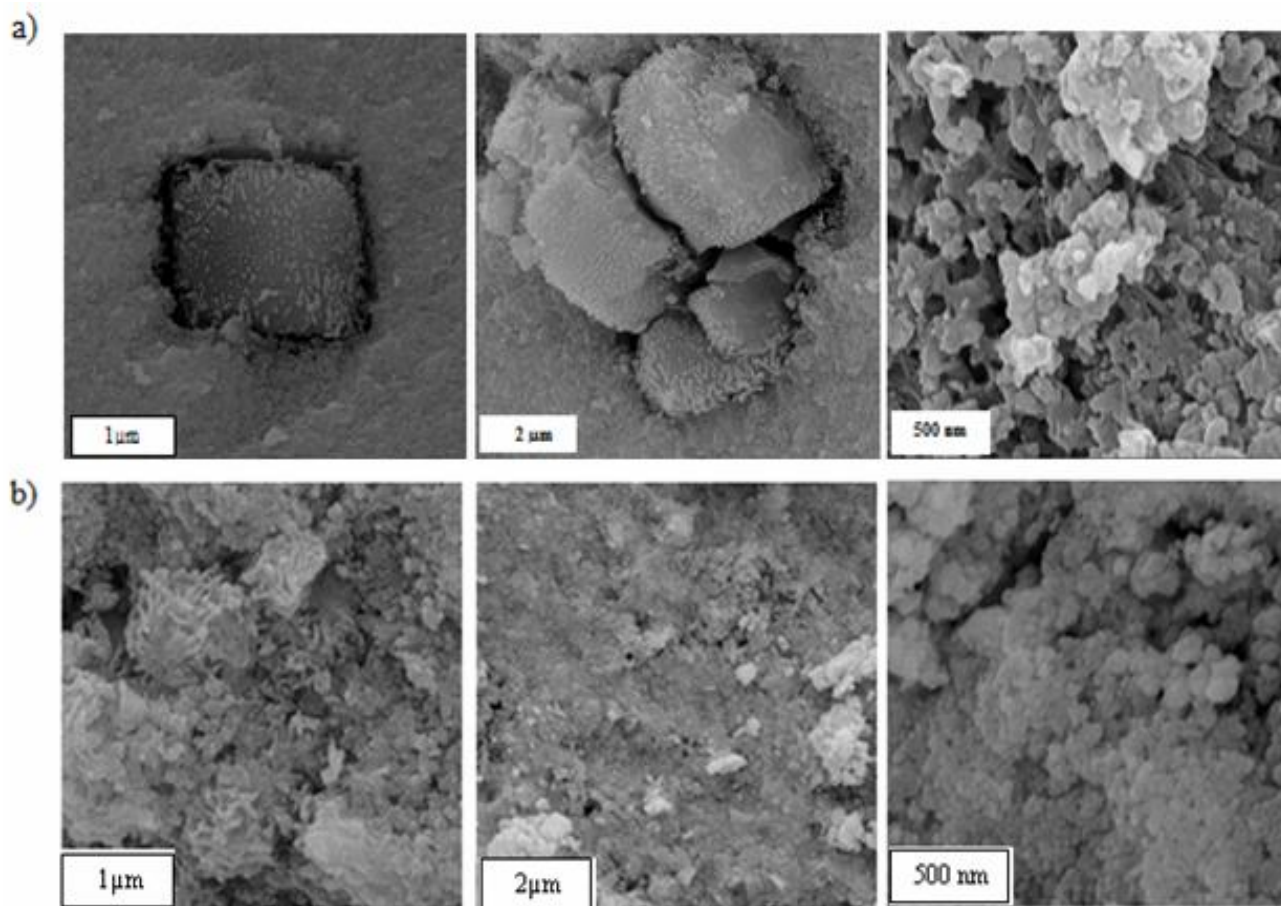


Fig. 6. SEM micrograph of a) L-CdS-NPs, and b) uncapped CdS-NPs.

Particle size distribution obtained from dynamic light scattering (DLS) for nanomaterial is shown in Fig. 8. The average particle size obtained from DLS data for dispersed nanomaterials in DMSO solvent give an average particle size of 87 nm for L-Ag-NPS (Fig. 8a) and 461 nm for L-CdS-NPs (Fig. 8b) that are different from those observed in DMSO solvent by AFM (86 and 54 nm for L-Ag-NPS and L-CdS-NPs, respectively). Moreover, they are larger than the average particle size estimated by XRD and SEM, due to the agglomeration of nanoparticles. DLS measurements are strongly influenced by larger particles in the sample and do not have narrow size distributions. Especially, DLS analysis includes the ligand shell whereas in other analysis we can look at the only metallic core. Heterogeneous distribution of nanoparticles in the matrix of ligand can result from the adhesion of nanoparticles also the process of

drying of samples may be due to the aggregation.

The AFM was used for imaging the nanoparticles. For AFM analysis, an appropriate dispersed solution of nanoparticles in DMSO was prepared. Using this technique, height (z-direction) was used to determine nanoparticle diameter (86 nm for Ag-NPS and 54 nm for CdS-NPs) as illustrated in (Fig. 9).

Fluorescence spectra of L, L-CdS-NPs, and uncapped CdS-NPs (Fig. 10) indicate that fluorescence of L-CdS-NPs is suppressed compared to L and bare CdS-NPs by a combination of inorganic nanoparticles with the organic ligands [36]. Since photoexcited electrons are transferred from the conduction band of CdS to the lowest unoccupied molecular orbital of ligand (LUMO), it can modulate the emission behavior of CdS [37].

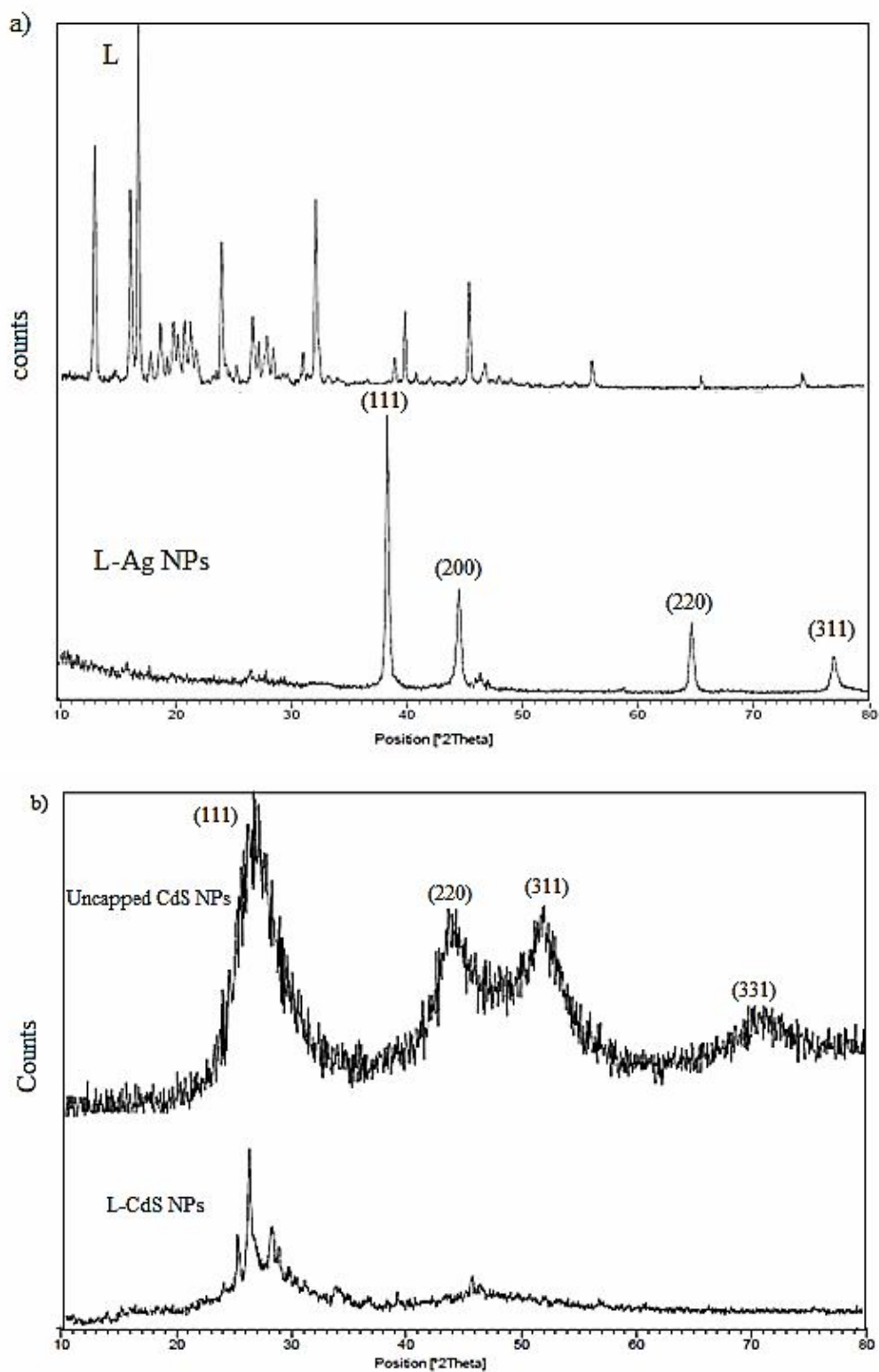


Fig. 7. The XRD patterns of a) L, L-Ag-NPs, b) L-CdS-NPs and uncapped CdS-NPs.

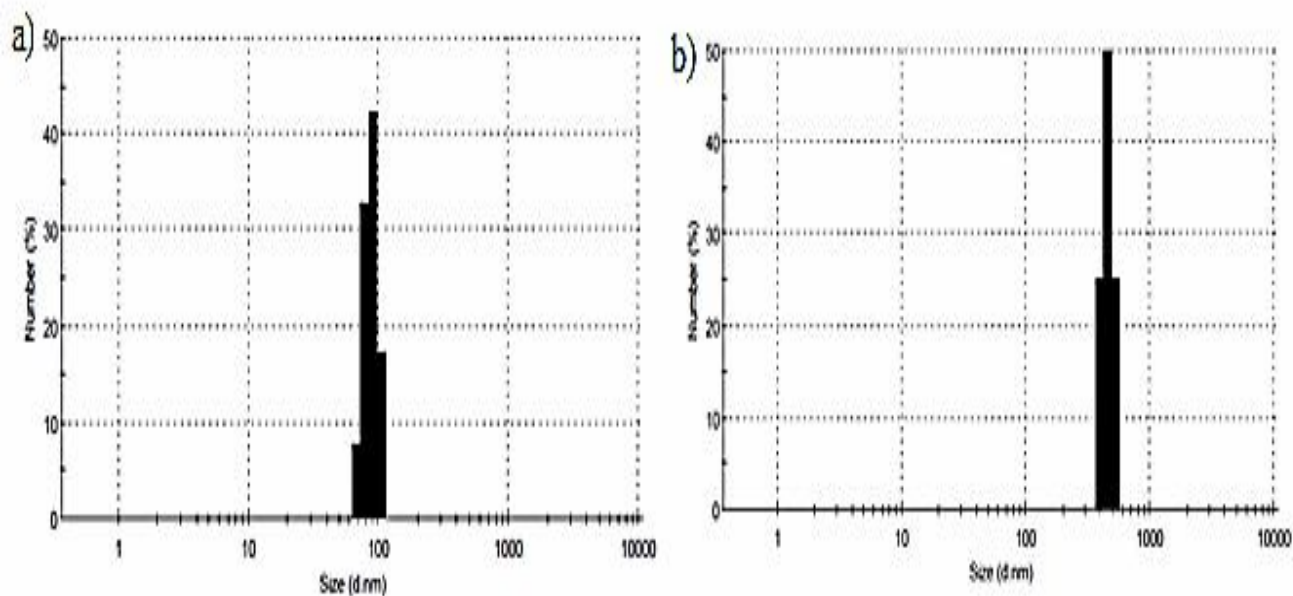


Fig. 8. DLS diagram of a) L-Ag-NPs, and b) L-CdS-NPs.

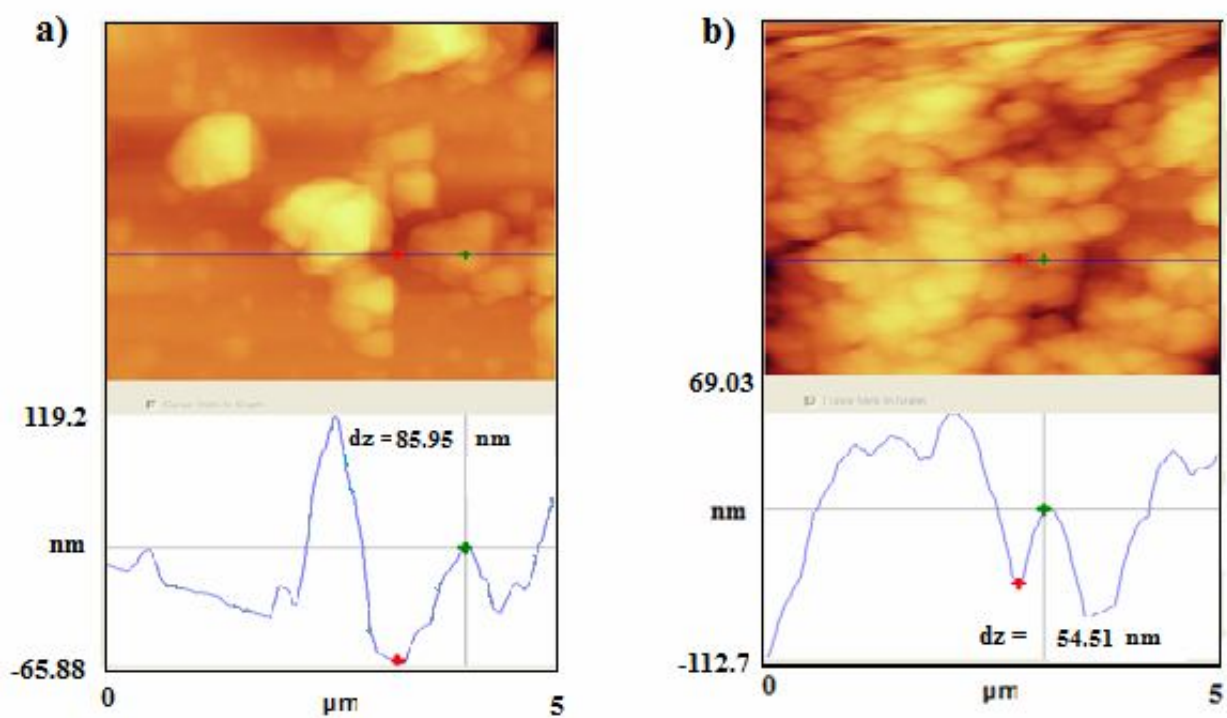


Fig. 9. AFM images of a) L-Ag-NPs and b) L-CdS-NPs.

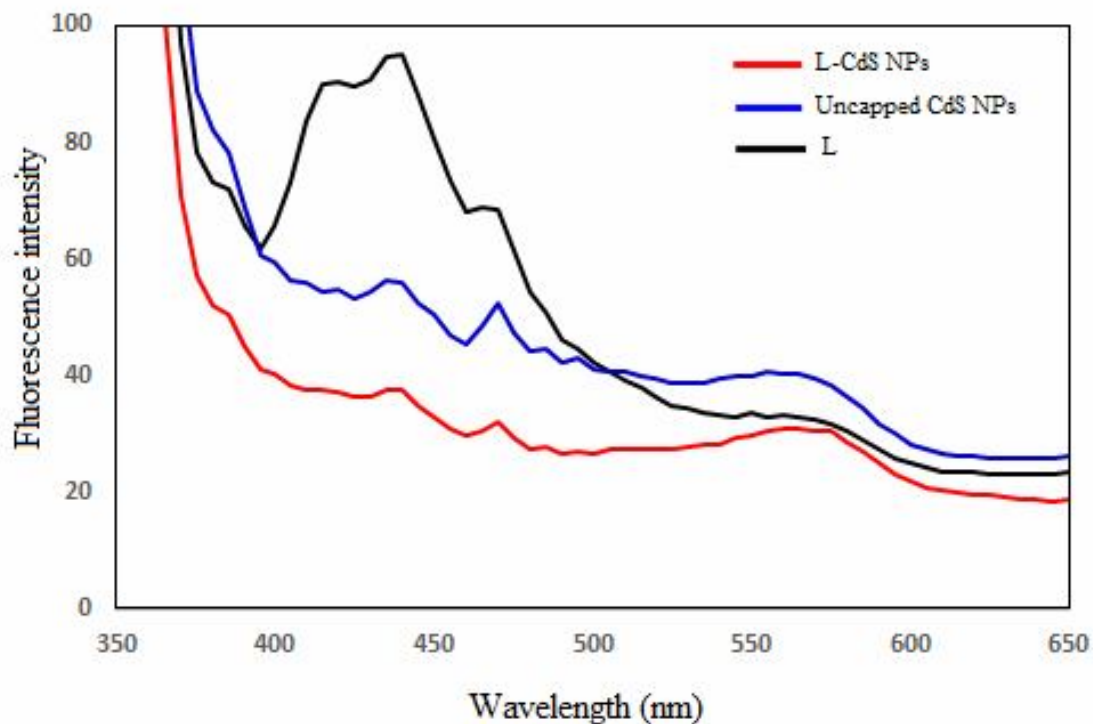


Fig. 10. Fluorescence image of L, L-CdS-NPs and uncapped CdS-NPs.

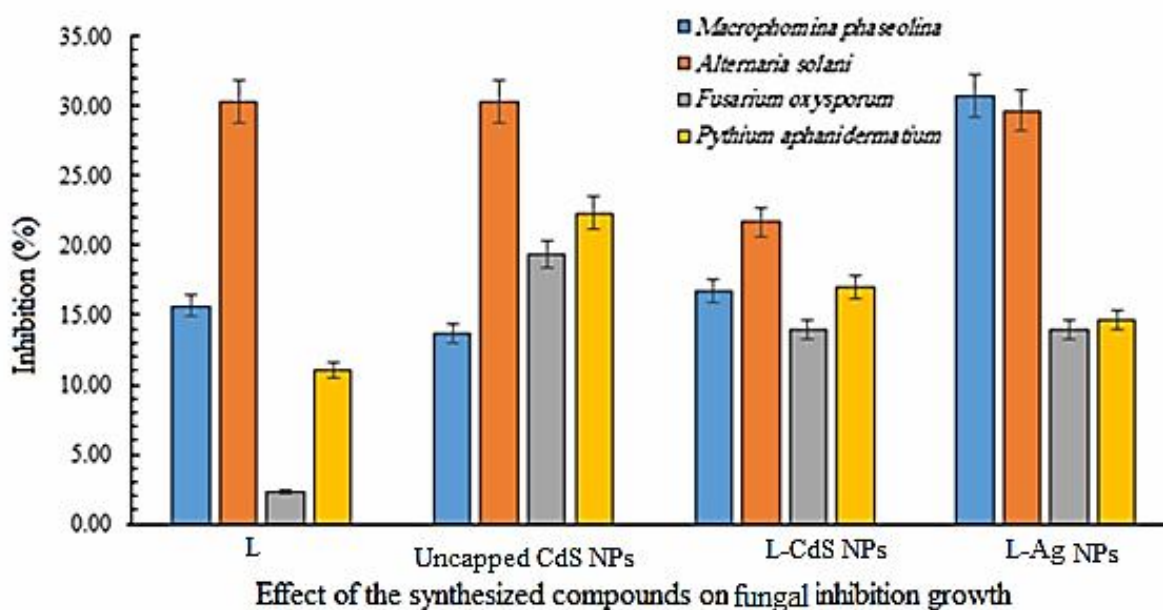
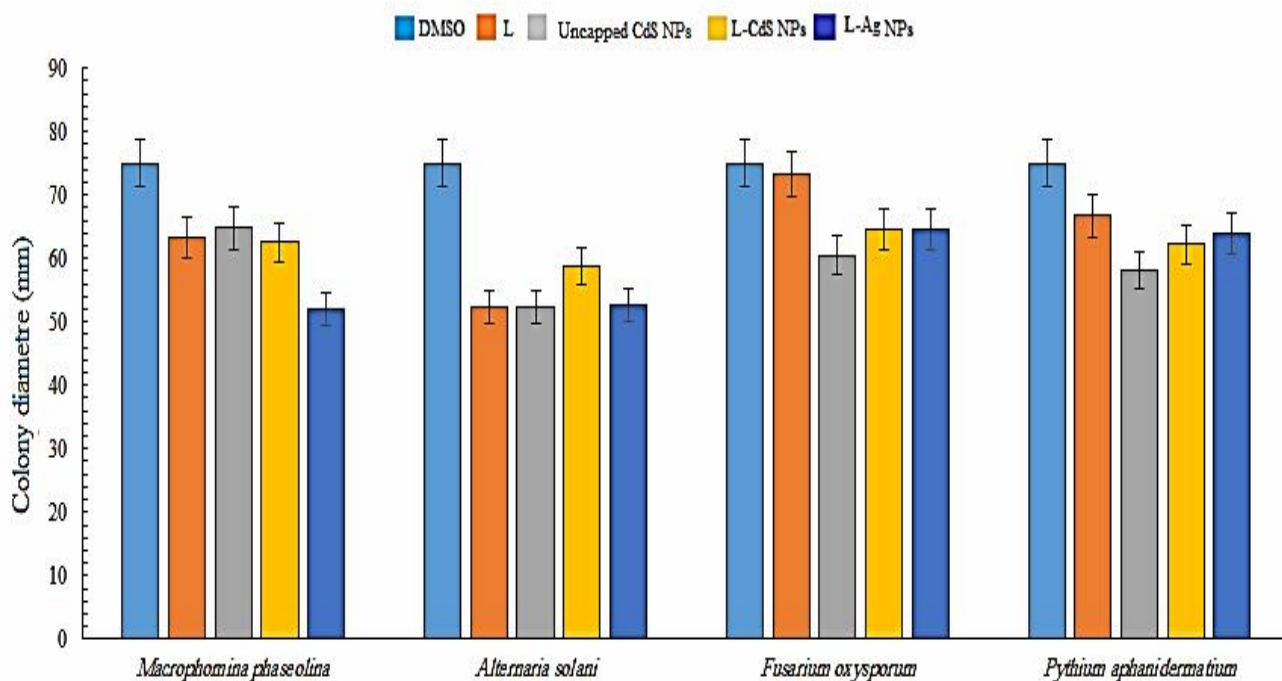


Fig. 11. Effect of the synthesized compounds on fungal inhibition growth.



Effect of the synthesized compounds on fungal colony growth

Fig. 12. Effect of the synthesized compounds on fungal colony growth.**Table 1.** *In vitro* Antibacterial Activity of L and L-Ag-NPs by

Compound	Inhibition zone (mm)			
	<i>S. aureus</i>	<i>B. cereus</i>	<i>E. coli</i>	<i>K. pneumonia</i>
L	19	-	-	-
L-Ag-NPs	20	16	11	12
DMSO	-	-	-	-
Amikacin (30 $\mu\text{g ml}^{-1}$)	25	14	24	22

Antibacterial and Antifungal Activities

Antibacterial and antifungal properties of the prepared materials were examined against different bacteria strains and four fungi. The sensitivity of L-Ag-NPs for bacteria was determined using well diffusion method while paper

disk method was used for L-CdS-NPs [26,27]. Growth inhibition percentage of the fungi was also determined. The results of antibacterial properties are presented in (Tables 1 and 2) and (Fig. S9). The results of antifungal activities are also listed in (Tables 3-5), (Figs. 11,

Table 2. *In vitro* Antibacterial Activity of L, L-CdS-NPs and Uncapped CdS by Disk Diffusion Method

Compound (30 $\mu\text{g mL}^{-1}$)	Inhibition zone (mm)			
	<i>S. aureus</i>	<i>B. cereus</i>	<i>E. coli</i>	<i>K. pneumonia</i>
	L	9	-	-
L-CdS-NPs	-	11	10	-
Uncapped CdS-NPs	-	-	-	-
DMSO	-	-	-	-
Amikacin	16	20	31	15

Table 3. Analysis of Variance of the Antifungal Effects of the Synthesized Compounds

P-value	value -F	Mean squares (MS)		Sum of squares (SS)		Degree of freedom(DF)			Coefficient changes (%)	Source of changes
		Error	Treatment	Error	Treatment	Total	Error	Treatment		
		0.0001	48.85**	1.83	156.30	22	625.20	19		
0.0001	39.55**	5.91	383.05	71	1532.20	19	12	4	4.18	<i>Alternaria solani</i>
0.0012	28.64**	3.21	156.88	38.5	627.5	19	12	4	2.75	<i>Pythium aphanidermatum</i>
0.0001	52.88**	2.89	276.13	34.70	1068.50	19	12	4	2.67	<i>Macrophomina phaseolina</i>

Where, * $p < 0.05$, ** $p < 0.01$ and *** $p < 0.001$ are level significant and $p > 0.05$ is insignificant.

12 and S10). The results show a difference among all compounds in terms of antibacterial activity. It was found that L-Ag-NPs has a moderate to high activity against both Gram-positives and Gram-negatives, however, L has low antibacterial activity. It has been shown that the Gram-negative bacteria are more sensitive to the Ag-NPs than Gram-positives that is probably due to the thick membrane of Gram-positives. This layer possesses linear

polysaccharide chains cross-linked by more short peptides and forms a complex structure that makes it difficult for Ag-NPs to penetrate Gram-positive bacteria. The cell membrane of bacteria consists of proteins containing sulfur, and the Ag-NPs interact with these proteins as well as the phosphorus-containing compounds like DNA. The nanoparticles cause structural changes in the bacterial cell wall and nuclear membrane ultimately leading to cell

Table 4. Comparison of Antifungal Activity of the Synthesized Compounds on Colony Growth

Colony growth (mm)				
<i>Macrophomina phaseolina</i>	<i>Altarnaria solani</i>	<i>Pythium aphanidermatium</i>	<i>Fusarium oxysporum</i>	Treatment
75 ^a	75 ^a	75 ^a	75 ^a	DMSO
63.25 ^b	52.25 ^c	66.75 ^b	73.25 ^a	L
64.75 ^b	52.25 ^c	58.25 ^d	60.50 ^c	Uncapped CdS-NPs
62.50 ^b	58.75 ^b	62.25 ^c	64.50 ^b	L-CdS-NPs
52 ^c	52.75 ^c	64.00 ^{bc}	64.50 ^b	L- Ag-NPs

Table 5. Antifungal Activity of the Synthesized Compounds

Inhibition (%)				
<i>Macrophomina phaseolina</i>	<i>Altarnaria solani</i>	<i>Pythium aphanidermatium</i>	<i>Fusarium oxysporum</i>	Treatment
0	0	0	0	DMSO
15.67	30.33	11	2.33	L
13.67	30.33	22.33	19.33	Uncapped CdS-NPs
16.67	21.67	17	14	L-CdS-NPs
30.67	29.67	14.67	14	L-Ag-NPs

distortion and death [38]. The synthesized L-Ag- NPs have antibacterial activity against different bacteria, and their effect on Gram-positives was stronger than Gram-negatives. L-CdS-NPs showed a moderate activity against *B. cereus* and *E. coli*. Nanometric dimensions of L-CdS-NPs allowed expansion of the contact surface of nanoparticles with the organism. Reports in the literature exhibit that electrostatic attraction between nanoparticles and bacterial cell walls is crucial for the activity of nanoparticles [39]. For L-CdS-

NPs, the higher activity compared to the free ligand may be related to chelation of the metal ion with donor atoms of the ligand [40] that reduces polarity of the metal ion. As a result, an increase occurs in the lipophilic character, favoring the permeation through lipid layers of the bacterial membrane that damages the outer cell membrane and consequently inhibits the growth of bacteria.

Among the mentioned compounds, L-Ag-NPs with 30.67 inhibition percentage against *Macrophomina*.

phasolina had the greatest inhibition effect. Uncapped CdS-NPs showed the greatest effect compared to the other compounds for all fungi except *M. phaseolina*. The antifungal activity against *A. solani* with 30.33% inhibition did not exhibit significant differences with L-Ag-NPs treatment and these two treatments were the best treatments on *A. solani*. After uncapped CdS-NPs, L-CdS-NPs had the greatest effect with 17% inhibition against *P. aphanidermatium*. Finally, following the uncapped CdS, NPs, L-CdS-NPs and L-Ag-NPs with 14% inhibition had the greatest effect on *F. oxysporum* and showed a significant difference. Among the tested fungi, *A. solani* had the most and *F. oxysporum* had the least sensitive fungus to the synthesized compounds (Tables 3-5).

CONCLUSIONS

Rational design, synthesis, characterization, and evaluation of antibacterial and antifungal properties of the azo-Schiff base (L), L-CdS-NPs, and L-Ag-NPs were accomplished. The obtained results in this study show that the methods used for the synthesis of nanostructures are simple and do not need long reaction times. The average sizes of nanomaterials were about 28-30 nm using the XRD technique. The XRD shapes exhibited a highly crystalline structure for L-Ag-NPs. Azo-Schiff base structure has a key role in the reaction process, reductive properties of OH groups and presence of donor atoms in ligand accelerate the formation of nanoparticles effectively. The study of fluorescence of cadmium sulfide nanoparticles indicates that fluorescence of L-CdS-NPs is suppressed compared to bare CdS-NPs and L. The samples were examined for antibacterial and antifungal activities against various pathogenic strains. The resulting NPs exhibited moderate to high activity against various microorganisms. We believe that the present work can open up a new and promising insight in the course of rational design, synthesis and applications of task-specific azo-Schiff base (L) for various purposes.

ACKNOWLEDGMENTS

We are grateful to the Lorestan University for financial support of this work.

REFERENCES

- [1] A.S. Gaballa, M.S. Asker, A.S. Barakat, S.M. Teleb, *Spectrochim. Acta, Part A: Mol. Biomol. Spectroscopy* 67 (2007) 114.
- [2] L. Shi, H.-M. Ge, S.-H. Tan, H.-Q. Li, Y.-C. Song, H.-L. Zhu, R.-X. Tan, *Eur. J. Med. Chem.* 42 (2007) 558.
- [3] D. Ayodhya, M. Venkatesham, A.S. Kumari, G.B. Reddy, D. Ramakrishna, G. Veerabhadram, *J. Fluorescence* 25 (2015) 1481.
- [4] E.E. Elemike, E.O. Dare, I.D. Samuel, J.C. Onwuka, *J. Appl. Res. Technol.* 14 (2016) 38.
- [5] I. Brigger, C. Dubernet, P. Couvreur, *Adv. Drug Deliv. Rev.* 54 (2002) 631.
- [6] X. Wu, H. Liu, J. Liu, K.N. Haley, J.A. Treadway, J. P. Larson, N. Ge, F. Peale, M.P. Bruchez, *Nat. Biotechnol.* 21 (2003) 41.
- [7] K.-J. Kim, W.S. Sung, B.K. Suh, S.-K. Moon, J.-S. Choi, J. G. Kim, D. G. Lee, *Biomaterials* 22 (2009) 235.
- [8] K.-H. Cho, J.-E. Park, T. Osaka, S.-G. Park, *Electrochim. Acta* 51 (2005) 956.
- [9] C.-N. Lok, C.-M. Ho, R. Chen, Q.-Y. He, W.-Y. Yu, H. Sun, P.K.-H. Tam, J.-F. Chiu, C.-M. Che, *JBIC J. Biol. Inorg. Chem.* 12 (2007) 527.
- [10] C. Aymonier, U. Schlotterbeck, L. Antonietti, P. Zacharias, R. Thomann, J.C. Tiller, S. Mecking, *Chem. Commun.* (2002) 3018.
- [11] A. Pal, S. Shah, S. Devi, *Colloids and Surf. A: Physicochem. Engin. Aspects* 302 (2007) 51.
- [12] M.T. Reetz, W. Helbig, *J. Am. Chem. Soc.* 116 (1994) 7401.
- [13] K.S. Suslick, S.-B. Choe, A.A. Cichowlas, M.W. Grinstaff, *Nature* 353 (1991) 414.
- [14] A. Pal, S. Shah, S. Devi, *Mater. Chem. Phys.* 114 (2009) 530.
- [15] H.J. Hah, S.M. Koo, S.H. Lee, *J. Sol-gel Sci. Technol.* 26 (2003) 467.
- [16] M. Pileni, *Langmuir* 13 (1997) 3266.
- [17] Y. Wang, C. To, D.H. Ng, *Mate. Lett.* 60 (2006) 1151.
- [18] W. Qingqing, X. Gang, H. Gaorong, *J. Solid State Chem.* 178 (2005) 2680.
- [19] N. Ushakov, G.Y. Yurkov, K. Zapsis, D. Baranov, N. Kataeva, I. Kosobudskiĭ, S. Gubin, *Optics and*

- Spectroscopy 100 (2006) 414.
- [20] P. Sharma, S. Brown, G. Walter, S. Santra, B. Moudgil, *Adv. Colloid Interface Sci.* 123 (2006) 471.
- [21] S. Omid, A. Kakanejadifard, F. Azarbani, *J. Mol. Liq.* 242 (2017) 812.
- [22] S. Boroon, A. Kakanejadifard, H. Motamedi, *J. Mol. Liq.* (2017).
- [23] A. Kakanejadifard, F. Azarbani, A. Zabardasti, S. Kakanejadifard, M. Ghasemian, F. Esna-ashari, S. Omid, S. Shirali, M. Rafieefar, *Dyes and Pigments* 97 (2013) 215.
- [24] M. Ghasemian, A. Kakanejadifard, F. Azarbani, A. Zabardasti, S. Kakanejadifard, *Petrochim. Acta, Part A: Mol. Biomol. Spectroscopy* 124 (2014) 153.
- [25] M. Ghasemian, A. Kakanejadifard, F. Azarbani, A. Zabardasti, S. Kakanejadifard, *J. Mol. Liq.* 195 (2014) 35.
- [26] L. Boyanova, G. Gergova, R. Nikolov, S. Derejian, E. Lazarova, N. Katsarov, I. Mitov, Z. Krastev, *J. Med. Microbiol.* 54 (2005) 481.
- [27] A. Bauer, W. Kirby, J.C. Sherris, M. Turck, *Am. J. Clin. Pathol.* 45 (1966) 493.
- [28] S. Tawata, S. Taira, N. Kobamoto, J. Zhu, M. Ishihara, S. Toyama, *Biosci., Biotechnol., Biochem.* 60 (1996) 909.
- [29] G. Singh, S. Maurya, M. De Lampasona, C.A. Catalan, *Flavour and Fragrance J.* 21 (2006) 472.
- [30] A. Kakanejadifard, F. Esna-ashari, P. Hashemi, A. Zabardasti, *Petrochim. Acta, Part A: Mol. Biomol. Spectroscopy* 106 (2013) 80.
- [31] A. Kakanejadifard, F. Azarbani, A. Zabardasti, A. Rezayat, M. Ghasemian, S. Kakanejadifard, *Petrochim. Acta, Part A: Mol. Biomol. Spectroscopy* 114 (2013) 404.
- [32] A. Kakanejadifard, F. Azarbani, Z. Saki, S. Kakanejadifard, A. Zabardasti, *Petrochim. Acta, Part A: Mol. Biomol. Spectroscopy* 132 (2014) 700.
- [33] M. Ghasemian, A. Kakanejadifard, T. Karami, *Spectrochim. Acta, Part A: Mol. Biomol. Spectroscopy* 168 (2016) 190.
- [34] M. Sahu, P. Biswas, *Nanoscale Res. Lett.* 6 (2011) 441.
- [35] P. Rodriguez, N. Munoz-Aguirre, E.S.-M. Martinez, G.G. de la Cruz, S. Tomas, O.Z. Angel, *J. Cryst. Growth* 310 (2008) 160.
- [36] T. Fukaminato, T. Sasaki, T. Kawai, N. Tamai, M. Irie, *J. Am. Chem. Soc.* 126 (2004) 14843.
- [37] A.A. Beharry, O. Sadovski, G.A. Woolley, *J. Am. Chem. Soc.* 133 (2011) 19684.
- [38] H. Song, K. Ko, I. Oh, B. Lee, *Eur. Cells Mater.* 11 (2006) 58.
- [39] A. Osowole, G. Kolawole, O. Fagade, *J. Coord. Chem.* 61 (2008) 1046.
- [40] P.K. Stoimenov, R.L. Klinger, G.L. Marchin, K.J. Klabunde, *Langmuir* 18 (2002) 6679.